INVESTIGATION OF THE TRANSONIC DRAG CHARACTERISTICS FOR NON-SLENDER WING-BODY COMBINATIONS AND THEIR EQUIVALENT AXISYMMETRIC BODIES AT ZERO LIFT

N. Agrell, R. Mattsson and S.-E. Nyberg
The Aeronautical Research Institute of Sweden (FFA)
S-161 11 Bromma, Sweden

ABSTRACT

A theoretical and experimental investigation was conducted to explore the applicability of the transonic similarity concept and also of the transonic area-rule for non-slender wing-body combinations. A family of eight wing-body combinations (wing aspect ratios 3-5) and their equivalent axisymmetric bodies were investigated at zero lift.

The transonic drag was determined by wind tunnel tests and by theoretical calculations using a transonic small disturbance method. The theoretical and experimental results for these non-slender configurations deviated from the transonic area-rule as the span increased, but confirmed the transonic similarity concept.

SYMBOLS

A	aspect ratio $\frac{b^2}{S_0}$
b	wing span
c	chord length
$\bar{c}$	mean chord
c_{ref}	mean aerodynamic chord $c_{ref} = 0.1055$ m
C_D	zero-lift drag coefficient $C_D = \frac{\text{Total drag - Base drag}}{q \cdot S}$
c_D	wing sectional drag coefficient
$C_{D_{nose}}$	zero-lift drag coefficient with $C_{D_{nose}} = \frac{\text{Nose drag}}{q \cdot S}$
C_{D_0}	zero-lift drag coefficient with wing area as reference area $C_{D_0} = \frac{\text{Total drag - Base drag}}{q \cdot S_0}$
$C_{D_{M=0.85}}$	zero-lift drag coefficient at M = 0.85
ΔC_D	$\Delta C_D = C_D - C_{D_{M=0.85}}$ (maximum cross sectional area as reference area)
ΔC_{D_0}	$\Delta C_{D_0} = C_{D_0} - C_{D_{0\,M=0.85}}$ (wing area as reference area)
$\Delta C_D'$	$\Delta C_D' = C_D - C_{D_{nose}} - C_{D_{M=0.85}}$
$\Delta C_{D_{nose}}$	$\Delta C_{D_{nose}} = C_{D_{nose}} - C_{D_{nose\,M=0.85}}$
C_p	pressure coefficient
f	body surface $z = f(x,y)$
M_∞	free stream Mach number
$\vec{n}$	unit vector normal to body surface
q	free stream dynamic pressure
r	radius of a body section
R	radius of computational cylinder
Re	Reynolds number based on $c_{ref} = 0.1055$ m
S	maximum cross sectional area
S_0	wing planform area, including portion within body
S_1	cross sectional area at station X_1
t	maximum thickness of wing profile
U_∞	free stream velocity
$\vec{u}$	velocity
x,y,z	Cartesian coordinates
x_1	location of the end of the body nose
x_2	location of the end of the body
X_1	longitudinal coordinate, measured from body nose
α	angle of attack
δ	average wing thickness ratio
ϵ	perturbation parameter - scaling factor
λ	similarity parameter $\lambda = (1-M_\infty^2)/\tau^2 M_\infty^2$
θ	angle about x-axis from plane of symmetry
θ_w	see Figure 8
φ	perturbation velocity potential
ϕ	total velocity potential
τ	thickness ratio for the equivalent axisymmetric body = maximum body diameter/body length
η	2y/b spanwise coordinate
η_{body}	spanwise location of wing-body junction

INTRODUCTION

When the experimental part of this investigation was conceived about three years ago, there was no suitable method available in Sweden for accurate calculation of the transonic drag characteristics for wing-body combinations. The main interest concerned at that time swept wings with aspect ratios around 4. Wings with supercritical airfoils designed by computational methods for two-dimensional flow had been windtunnel tested, but the improvement in drag characteristics demonstrated in two-dimensional tests, did not come out in three-dimensional tests. It was obvious that more detailed insight had to be gained about three-dimensional transonic flow around swept wings of moderate aspect ratio.

One of the approaches to the three-dimensional flow problem was the experimental investigation reported in this paper. The purpose of the investigation was to explore the applicability and the limitations of a transonic similarity concept and also of the transonic equivalence rule for non-slender wing-body combinations at zero lift. A large number of investigations on the transonic similarity and equivalence rules have been carried out during the last three decades. Summaries with bibliographies of the most important work have been made for instance by Spreiter [1] and Oswatitsch [2,3]. Systematic experimental investigations have been made on the similarity rule among others by McDevitt [4] on wings with rectangular planform and by Page [5] on wings with triangular planform. The classical investigations of the area-rule by Whitcomb [6] dealt with thin triangular and swept wings of low aspect ratio. An investigation by Drougge [7] of the interference between bodies of revolution at transonic speeds accomplished important results with reference to the sonic and supersonic area rules as well as the transonic similarity rule. It appears however, that the validity of these concepts for wing-body combinations with fairly thick, moderately swept tapered wings of intermediate aspect ratios has not been explored. The present investigation was therefore conceived, to provide some test data for this kind of configurations, typical for advanced jet trainers and strike aircraft.

The basic configuration for the models investigated had a 35° swept wing with 8.9% thickness and an aspect ratio of 4 in mid-wing position on a cylindrical body with an ogive nose. Two affinely related wing-body combinations and their equivalent axisymmetric bodies were constructed for investigation of the transonic similarity rule for slender bodies [7,8]. The wings where also investigated in combination with bodies designed in accordance with the transonic area-rule [9]. In the area-rule investigation the wings were tested with two bodies, one having the axial area distribution of the basic configuration and one having a more favourable area distribution. The equivalent axisymmetric bodies for these configurations were also investigated. The tests covered drag measurements, flow studies and Schlieren photography.

While the experimental investigation was in progress, a theoretical three-dimensional relaxation method based on the transonic small disturbance equation was developed [10]. As soon as it was demonstrated that the method could be used also for calculation of transonic drag rise [11], it was decided to start a parallel theoretical investigation, using the transonic small disturbance method for drag calculations. All wing-body combinations tested have also been investigated theoretically but not the equivalent axisymmetric bodies. The reason is that the computational grid is adapted for wing-body calculations and is therefore not in its present form particularly suited for the calculation of flow around axisymmetric bodies alone. A special technique, developed to handle the computation of the "area-ruled" bodies, as well as the results of the calculations are described in the paper.

EXPERIMENTAL INVESTIGATION

Wind Tunnel

The experimental investigation was done in the FFA-HT transonic wind tunnel, which is of the continuous drive, closed circuit, variable pressure type [12]. The test section, which is 0.90 x 0.90 m^2 with octagonal cross section, is ventilated by shallow longitudinal slots, one in each corner. The open area of the slots is 9.2 %.

Models

Basic Model. The basic model designated PT5A is shown in Figure 1. It is a mid-wing version of a high-wing configuration PT1, which has been extensively tested at FFA and NAE [13,14].

The wing is a swept tapered wing with an aspect ratio of 4.0, taper ratio 0.4 and a sweep back angle of 35° on the 25 % chord line. The wing profile is NACA 64A010 perpendicular to the quarter-chord line, which gives a wing thickness ratio of 8.9 % in the free stream direction. The body consists of a circular cylinder with a tangent ogive pointed nose of fineness ratio 2.5.

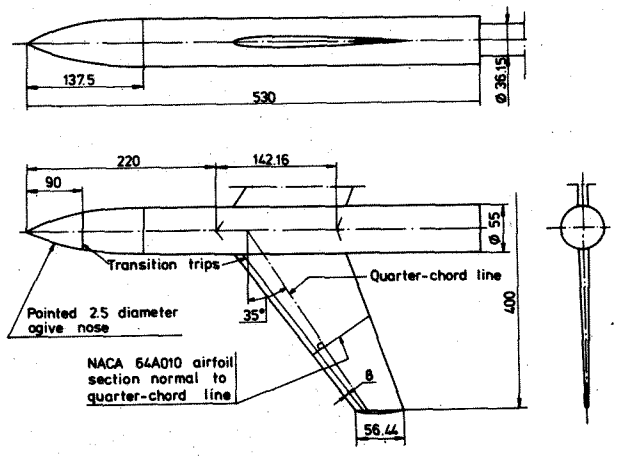

FIGURE 1. The basic model PT5A

Models for Similarity Rule Tests. Two wing-body combinations with geometry affinely related

to the basic configuration were obtained by scaling the model cross sections with radial scale factors of $\sqrt{0.6}$ and $\sqrt{1.4}$ respectively. The scale factors had to be limited in order to avoid steep area variations on the bodies for the area-rule models described later. The planforms of the models are shown in Figure 2. The model designated PT4A has a thinner wing of smaller span than the basic configuration while model PT6A has a thicker wing of larger span. Main data for the models are presented in Table 1. The sting diameter is scaled in accordance with the models.

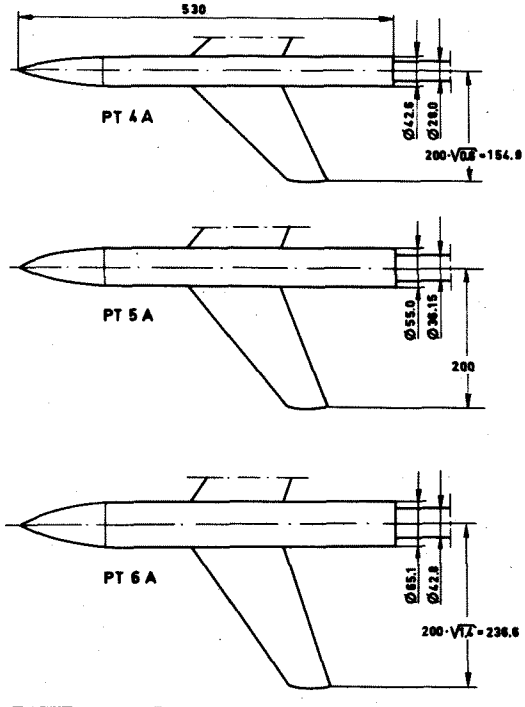

FIGURE 2. The affinely related wing-body models for testing the transonic similarity rule

The axial area distributions for these models are presented in Figure 3 and their equivalent axisymmetric models with stings are shown in Figure 4. The axisymmetric models have an R added to the designation, for instance PT4AR, etc. These models among themselves are clearly affinely related in accordance with the similarity rule.

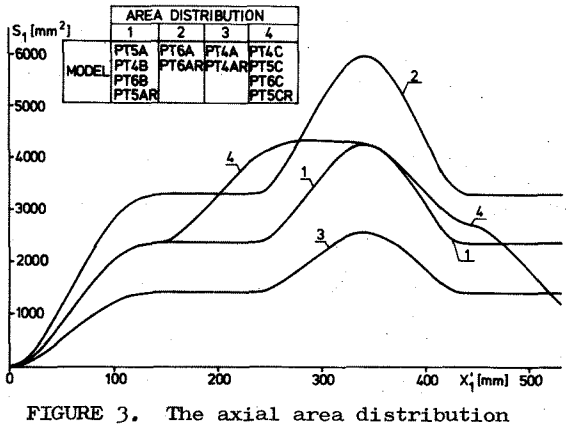

FIGURE 3. The axial area distribution for the models

	PT4A	PT5A	PT6A
Aspect ratio (A)	4.0 $\sqrt{0.6}$ = 3.10	4.00	4.0 $\sqrt{1.4}$ = 4.73
Max. wing thickness in free stream direction $(Hc)_{max}$	8.9 $\sqrt{0.6}$ = 6.9 %	8.9 %	8.9 $\sqrt{1.4}$ = 10.5 %
Sweep angle at quarter-chord line	42°1	35°0	30°6
Relative thickness for equivalent body of revolution (τ)	13.91 $\sqrt{0.6}$ = 10.77 %	13.91 %	13.91 $\sqrt{1.4}$ = 16.45 %
Wing area (S_o, cm²)	307.7	397.2	470.0
Max. cross sectional area (S cm²)	25.59	42.66	59.72

TABLE 1. Certain data for the three affinely related models

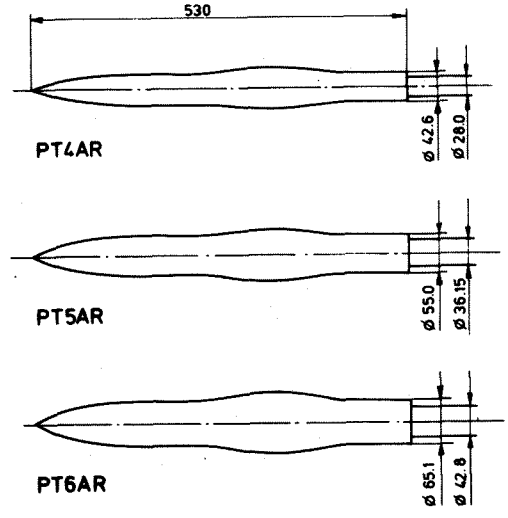

FIGURE 4. The affinely related axisymmetric bodies area equivalent to the models in Figure 2

Models for Area-Rule Tests. The wings of the models PT4A and PT6A could also be combined with bodies designed in accordance with the transonic area-rule in such a way that these configurations have the same axial area distribution as PT5A (area distribution 1 in Figure 3). The compensation for the differences in the cross sectional area of the wings is made by varying the diameter of the body, which for each model is a body of revolution. The models, denoted PT4B and PT6B, are depicted in Figure 5 together with the area-equivalent models PT5A and PT5AR.

All three wings could also be combined with another set of bodies designed in the same way to correspond to a common, more favourable area-distribution (distribution 4 in Figure 3). These models, denoted PT4C, PT5C and PT6C, as well as their equivalent axisymmetric body PT5CR are presented in Figure 6.

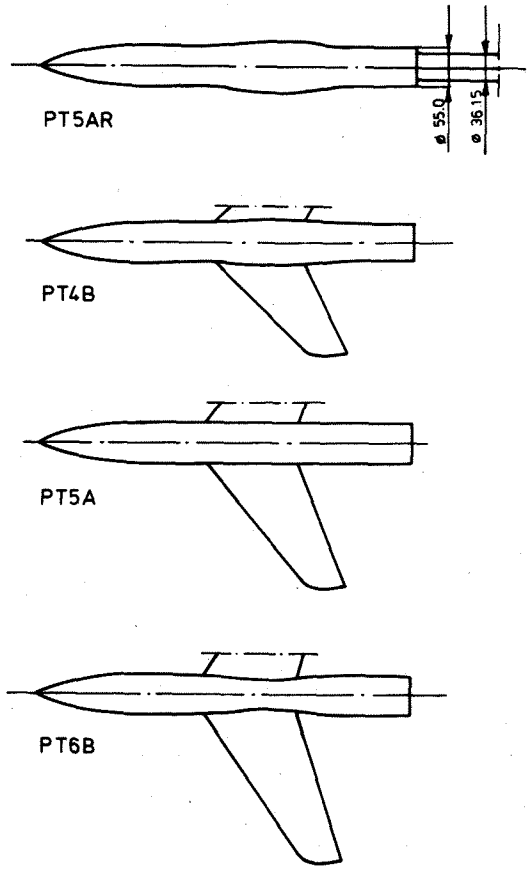

FIGURE 5. The models with axial area distribution 1 for area-rule tests

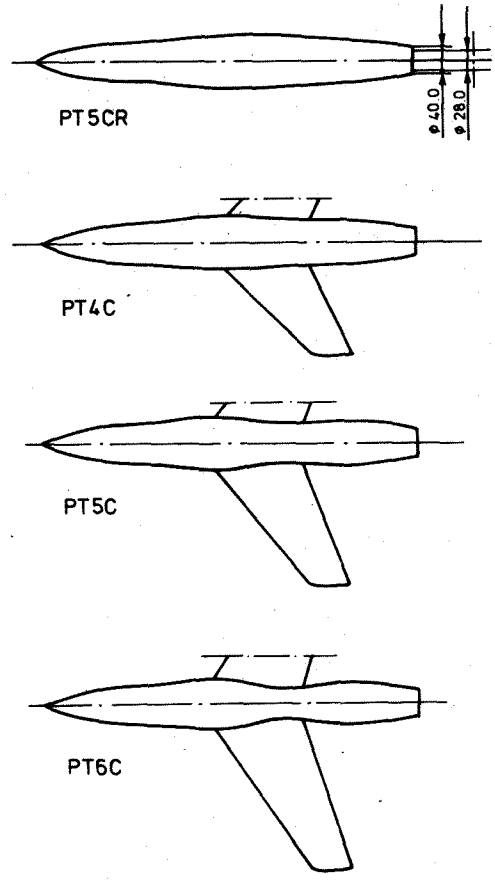

FIGURE 6. The models with axial area distribution 4 for area-rule tests

Tests

To ensure fixed transition in all tests and a turbulent boundary layer where shocks occur the models had transition trips consisting of 0.2 mm diameter steel balls with 4 mm spacing welded to the models close to the wing leading edges and on the body nose as shown in Figure 1.

The test programme consisted of three-component force measurements and measurement of the base pressure for in all 12 model configurations in the Mach number range 0.5 - 1.05 at a constant Reynolds' number based on reference chord $c_{ref} = 0.1055\,m$ $Re = 1.0 \cdot 10^6$. The angle of attack was varied within the range $\alpha = \pm 5^o$ for the wing-body configurations and $\alpha = \pm 2^o$ for the axisymmetric bodies. The results presented in this paper however cover only the zero-lift case.

The test Mach numbers were selected to achieve test results at given values of the similarity parameter $\lambda = (1-M_\infty^2)/\tau^2 M_\infty^2$, where τ is the thickness ratio of the equivalent axisymmetric body. The test programme is shown in Table 2.

Schlieren photographs were taken at most test conditions and oil flow studies were made in some selected cases.

	PT4A PT4AR	PT5A PT4B PT6B PT5AR	PT6A PT6AR	PT5C PT4C PT6C PT5CR
	$\tau = 0.1077$	$\tau = 0.1391$	$\tau = 0.1645$	$\tau = 0.1409$
λ	M'	M'	M'	M'
110	0.663	0.565	0.501	0.561
70	0.743	0.652	0.588	0.647
40	0.826	0.751	0.693	0.747
30	0.861	0.795	0.743	0.792
20	0.901	0.849	0.806	0.846
16	0.918	0.874	0.835	0.871
12	0.937	0.901	0.869	0.899
10	0.947	0.915	0.887	0.914
8	0.957	0.931	0.907	0.929
6	0.967	0.947	0.928	0.945
4.5	0.975	0.959	0.944	0.958
3.0	0.983	0.972	0.962	0.972
2.0	0.989	0.981	0.974	0.981
1.0	0.994	0.990	0.987	0.990
0.0	1.000	1.000	1.000	1.000
- 0.75	-	-	1.010	-
- 1.75	1.010	1.017	1.025	1.018
- 3.5	1.021	1.036	-	1.037
- 5.0	1.030	1.052	-	1.054
- 6.5	1.040	-	-	-

TABLE 2. Test programme

Corrections to Test Data

All drag coefficients obtained from the wind tunnel tests are presented with the measured base drag subtracted. No corrections for wind tunnel wall interference have been applied.

For correlations with the similarity concept and for comparisons with theoretical calculations the pressure drag coefficient is required. This is obtained by subtracting the friction drag coefficient from the drag coefficient C_D determined by the force measurements. It has been assumed that the friction drag coefficient changes negligibly in the transonic range and that it can be approximated by the drag coefficient at Mach number $M_\infty = 0.85$. The drag rise coefficient ΔC_D used in correlations expresses the drag rise above the drag level at $M_\infty = 0.85$.

A further correction had to be applied to the experimental results before comparison with the theoretical calculations could be made. As the calculated drag does not include the nose drag, the experimental results were corrected by subtracting the estimated nose drag. The estimation was made by extrapolating the experimental pressure drag data for slender bodies of revolution investigated by Drougge [7] to the nose geometries of interest for our models. The estimated nose drag correction $\Delta C_{D_{nose}}$ as shown in Figure 7 is subtracted from the drag rise coefficient ΔC_D and a corrected drag rise coefficient $\Delta C_D'$ suitable for comparison with theoretical results is obtained. This method of correction seems reasonable for the A- and B-models, where the nose is followed by a circular cylinder. For the C-models, where the body cross sectional area increases smoothly downstream of the nose the method of correction seems more questionable, but has been accepted, as the corrections are small for Mach numbers $M_\infty < 0.94$ and the same for all models in the family.

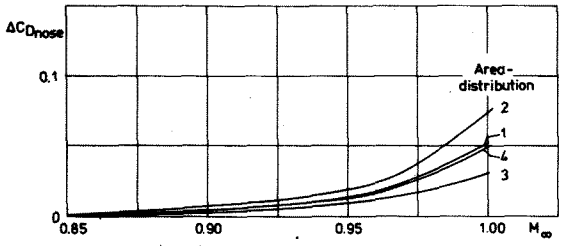

FIGURE 7. The estimated nose drag correction

THEORETICAL INVESTIGATION

Method of Calculation

The classical small-disturbance equation for the perturbation potential φ is given by

$$[(1-M_\infty^2) - (\gamma+1)\varepsilon M_\infty^2 \varphi_x]\varphi_{xx} + \varphi_{yy} + \varphi_{zz} = 0 \qquad (1)$$

where φ is defined in terms of the full velocity potential ϕ as

$$\phi(x,y,z) = U_\infty[x + \varepsilon\varphi(x,y,z)] \qquad (2)$$

with $\varepsilon = \delta^{2/3}/M_\infty$ and δ being a measure of relative wing thickness.

The velocity vector is given by (see Eq.(2))

$$\vec{u} = (\phi_x, \phi_y, \phi_z) = U_\infty(1 + \varepsilon\varphi_x, \varepsilon\varphi_y, \varepsilon\varphi_z) \qquad (3)$$

If the surface of the configuration to be treated is $z = f(x,y)$ the unit vector normal to any point on the configuration is given by

$$\vec{n} = \frac{1}{\sqrt{1+f_x^2+f_y^2}}(-f_x, -f_y, 1) \qquad (4)$$

Flow tangency condition at the surface can be expressed as

$$\vec{u} \cdot \vec{n} = 0 \qquad (5)$$

(3), (4) and (5) give us the boundary condition

$$\varphi_z = (\frac{1}{\varepsilon} + \varphi_x)f_x + \varphi_y f_y \qquad (6)$$

For small disturbances (6) can be simplified to

$$\varphi_z = \frac{1}{\varepsilon} f_x \qquad (7)$$

Assuming the wing to be thin (7) can be used as the boundary condition on the wing.

The computational body points do not coincide with the real points on the body. Correction was therefore made for the slopes when transferring them from the real to the computational body points. The slopes dr/dx were scaled with the ratio of the body radius r to the reference cylinder radius R. This is in accordance with the slender body theory as long as the angle of attack is zero.

To solve Eq.(1) the relaxation procedure introduced by Murman and Cole [15] has been used. The shock point operator [16] has been used throughout the computations. Details of the method can be found in Ref. [17].

The pressure coefficient C_p for isentropic potential flow is given by the relation

$$C_p = \frac{2}{\gamma M_\infty^2}\left\{\left[1 - \frac{\gamma-1}{2} M_\infty^2(2\varepsilon\varphi_x + \varepsilon^2(\varphi_x^2+\varphi_y^2+\varphi_z^2))\right]^{\frac{\gamma-1}{\gamma}} - 1\right\} \qquad (8)$$

The second order approximation of (8) gives

$$C_p = -\left\{2\varepsilon\varphi_x + \varepsilon^2\left[(1-M_\infty^2)\varphi_x^2 + \varphi_y^2 + \varphi_z^2\right]\right\} \qquad (9)$$

Expression (9) has been used to calculate pressure coefficients on the complete configuration.

Wing Drag Evaluation

Pressure coefficients are integrated in order to obtain the forces on the configuration. As the angle of attack is zero in the present investigation the drag evaluation is of great importance. The integration has first been performed around the wing contour at fixed spanwise location in order to obtain a measure of the drag $c_D(\eta)$ at each section.

$$c_D(\eta) = \oint C_p(z/c, \eta)\, d(z/c) \qquad (10)$$

Finally the integration was carried out over the span of the wing and the total drag is obtained from

$$C_D = \int_{\eta_{body}}^{1} \frac{c(\eta)}{\bar{c}} c_D(\eta) \cdot d\eta \qquad (11)$$

where

$$\bar{c} = \int_0^1 c(\eta)\, d\eta \qquad (12)$$

and $\eta = 2y/b$. The for the drag important leading edge pressure coefficient cannot be computed by small disturbance theory and simple sweep theory has been used to estimate it instead. For more detailed description of the drag evaluation on the wing see Ref.[11].

Body Drag Evaluation

Considering the fact that the nose region of the body is represented by few computational points it was decided not to try to evaluate the drag of the nose region from computed pressures but to estimate it from earlier experiments[7] and subtract it from the drag obtained by experiments in this investigation.

As the slopes (i.e. boundary conditions) have been corrected (see Method of Calculation) for the entire body and as the distances between the real body points and the corresponding computational points are considered to be small, except at the nose region, it can be assumed that the computed pressure coefficients are valid for the corresponding real body points. As the cross-sectional areas of the bodies investigated are circular, and as the wing is mid-mounted and symmetrical through the $z = 0$ plane and the angle of attack α is zero the integration needs to be performed only for one quadrant of the body section (see figure 8).

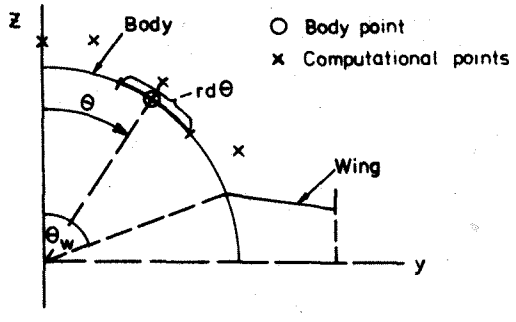

FIGURE 8. Geometry and computational points at wing-body junction

Multiplying the result by 4 and then integrating along the body (excluding the nose region) gives

$$C_{D_0} = \frac{4}{S_0} \int_{x=x_1}^{x=x_2} \int_{\theta=0}^{\theta=\theta_w} \left(r \frac{dr}{dx}\right) C_p(x,\theta) d\theta dx \qquad (13)$$

where

$$S_0 = \bar{c} \cdot b \qquad (14)$$

RESULTS AND DISCUSSION

Similarity Rule Investigation

Correlation Parameters. The affine models are related by constant radial scaling factors, which means that in each cross section of the wing the spanwise coordinate and the thickness are scaled by the same factor. This was done for the purpose of checking whether and if so within which range the transonic similarity rule for flow around slender bodies was applicable for this family of not-so-slender radially scaled wing-body combinations. The similarity rule for slender bodies[7,8] states that the wave drag is proportional to τ^2 and is a function of the parameter

$$\lambda = \frac{1-M_\infty^2}{M_\infty^2 \tau^2}$$

The wave drag is not measured directly, but is assumed to be approximated by the transonic drag rise. The correlation was therefore made by plotting

$$\Delta C_D/\tau^2 \text{ versus } \lambda$$

for the experimental investigation and

$$\Delta C_D'/\tau^2 \text{ versus } \lambda$$

for the theoretical investigation including comparison with corrected experimental results.

One attempt was also made to determine the range of applicability of the transonic area-rule by correlating the results in accordance with the transonic similarity rule for thin wings[5,18]. This was done by plotting

$$\frac{\Delta C_{D_0}}{(t/c)^{\frac{5}{3}}} \text{ versus } A(t/c)^{\frac{1}{3}}$$

Experimental Results. The basic characteristics of the measured zero-lift drag versus Mach number for the wing-body combinations are presented in Figure 9 and for the equivalent axisymmetric bodies in Figure 10[19]. It should be noted that the drag coefficient C_{D_0} shown in Figure 9 and the drag-rise coefficient ΔC_{D_0} in Figure 14 are evaluated with the wing planform area as reference area to indicate the drag levels in terms typical for aircraft aerodynamics, but for all other results presented in this paper the maximum cross sectional area is used as reference area.

The correlation of the transonic drag rise with the similarity rule parameter λ for all the affinely related models is presented in Figure 11. The correlation for the wing-body models is very good except for the PT6A model very close to $\lambda = 0$ ($M_\infty = 1.00$). This might be an effect of wind tunnel wall interference. The good correlation is nevertheless remarkable, as noticeable separations on the wing were observed at some Mach numbers during the flow visualization tests. In Figure 12 are depicted Schlieren and surface flow visualization pictures for $\lambda = 4.5$, where the separations were most severe. The Schlieren and oil flow pictures are enlarged to the same scale, so that direct comparisons

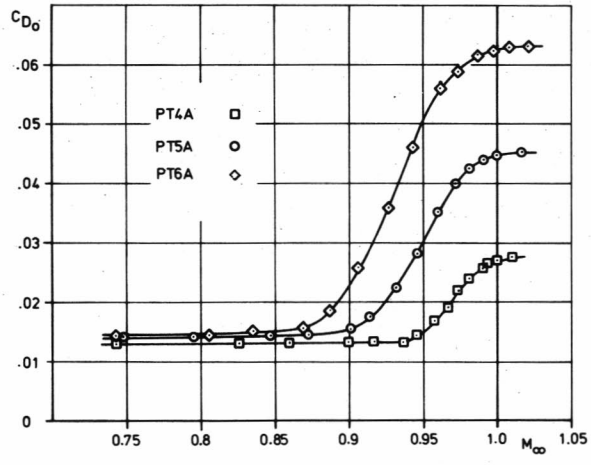

FIGURE 9. The zero-lift drag coefficient for PT4A, PT5A and PT6A with the wing area as reference area

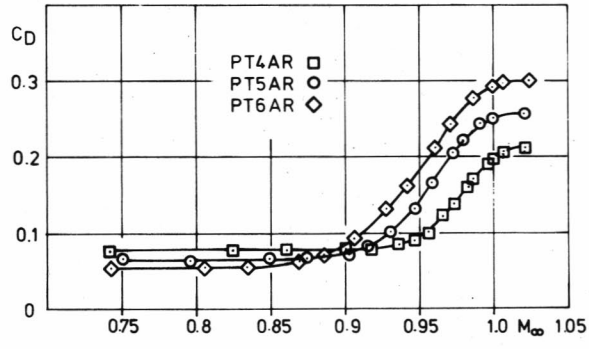

Figure 10. The zero-lift drag coefficient C_D for PT4AR, PT5AR and PT6AR

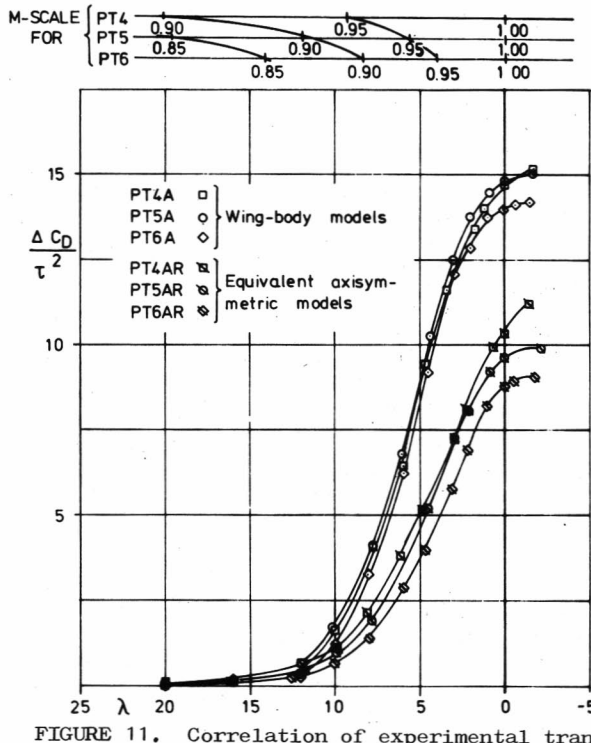

FIGURE 11. Correlation of experimental transonic drag rise for the affinely related models

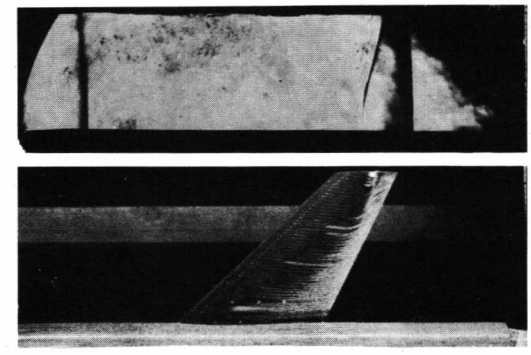

FIGURE 12a. PT4A $\lambda = 4.5$ $M_\infty = 0.975$

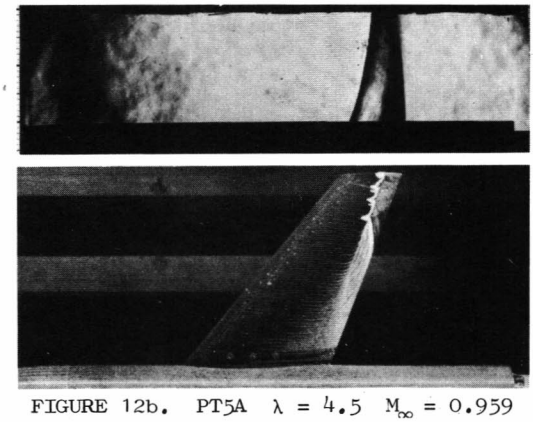

FIGURE 12b. PT5A $\lambda = 4.5$ $M_\infty = 0.959$

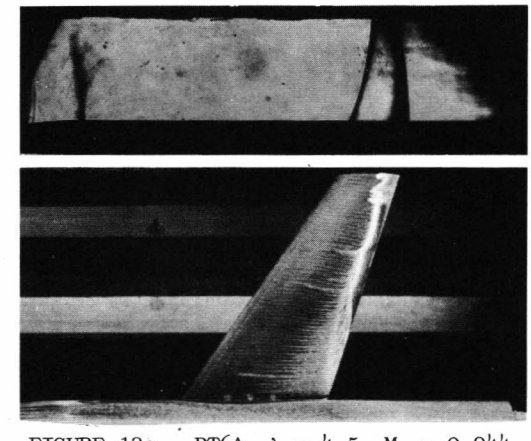

FIGURE 12c. PT6A $\lambda = 4.5$ $M_\infty = 0.944$

FIGURE 12. Schlieren and surface flow visualization pictures for the affinely related wing-body models at $\lambda = 4.5$

can be made between the shock positions and the separation for each model and also between the models. The shock positions and the separations are remarkably similar.

The correlation of the equivalent axisymmetric bodies in Figure 11 is reasonably good between PT4AR and PT5AR, but the PT6AR drops somewhat below. The surface flow visualization tests for the PT6AR revealed that in the entire λ range 0-10 there is a separated region with reversed flow at the downstream end of the bump, equivalent to the wing. An example can be seen in Figure 13, where PT5AR and PT6AR show separations with reversed flow, while PT4AR shows oil

paint accumulation in the same area but no indications of complete separation rather of intense boundary layer thickening. Broadly the same flow picture was found for PT4AR in the entire λ range and in some cases also for PT5AR, while this latter model in other cases showed separation.

From Figure 11 it is further obvious that the curves for the wing-body models are far from the curves for their equivalent axisymmetric bodies, so that already here it can be seen that the simple transonic area-rule is not valid for any of these configurations.

In Figure 14 is shown for the family of wing-body combinations the variation at sonic speed of the reduced drag-rise coefficient $\Delta C_{D_0}/(t/c)^{5/3}$ versus $A(t/c)^{1/3}$, the correlation parameter according to the transonic similarity rule for thin wings. In the same diagram are included for comparison previous test data for wings with rectangular [4] and triangular [5] planform. The figure shows that the data for PT4A and PT5A are on a straight line through the origin, while the curve deviates from this straight line at some value of $A(t/c)^{1/3}$ between the data points for PT5A and PT6A. It has been stated in earlier investigations [5,18], that when data plotted in a diagram of this kind correlate to a straight line through the origin, they are in accordance with the transonic area rule. This should imply that the test data for PT4A and PT5A are in accordance with the transonic area rule, but that the data for PT6A are not. This is contradicted by the results shown in Figure 11 and also by other results presented later in this paper, where it is inferred that the transonic area-rule is not valid at sonic speed for any of the wing-body combinations tested in this investigation.

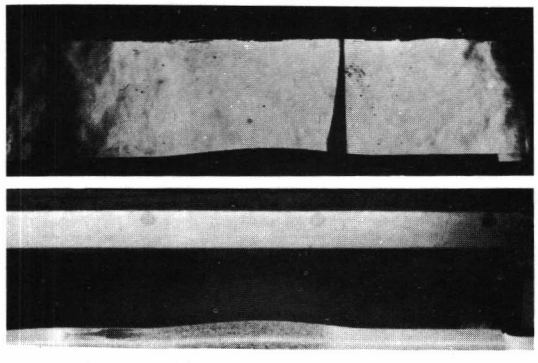

FIGURE 13a. PT4AR $\lambda = 3$ $M_\infty = 0.982$

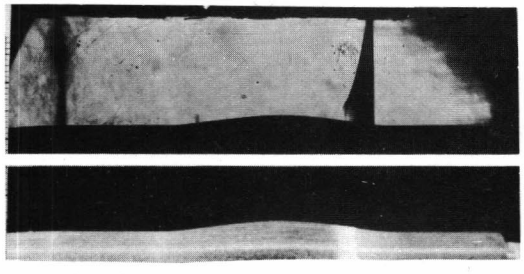

FIGURE 13b. PT5AR $\lambda = 4.5$ $M_\infty = 0.959$

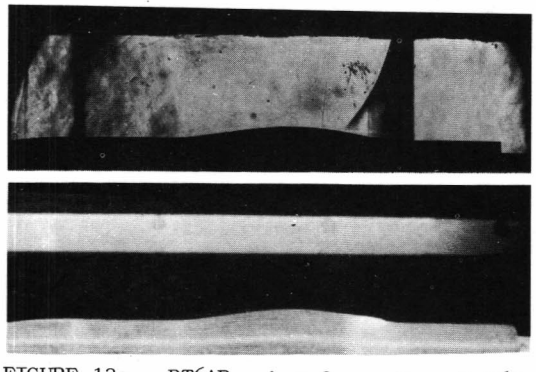

FIGURE 13c. PT6AR $\lambda = 3$ $M_\infty = 0.962$.

FIGURE 13. Schlieren and surface flow visualization pictures for the affinely related equivalent axisymmetric bodies at $\lambda = 3 - 4.5$

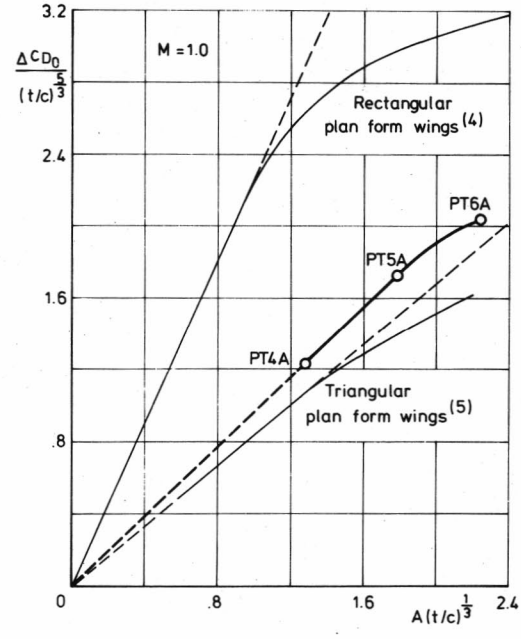

FIGURE 14. Comparison of the drag-rise at sonic speed for triangular and rectangular wings with the affinely related trapezoidal wing-body combinations

Theoretical Results and Comparison with Experiments. Computations have been carried out for Mach numbers .85, .90, .92 and .94 for all configurations except PT4A where Mach numbers .96 and .97 have been added. Convergence problems could clearly be seen at M = .97 which corresponds to quite low λ. The computational time is increasing considerably with increasing Mach number for each configuration and this fact together with convergence problems for low λ's decided the upper Mach number limit for the computations.

Shown in Figure 15 is the variation of the calculated drag-rise coefficient $\Delta C_D'$ (nose

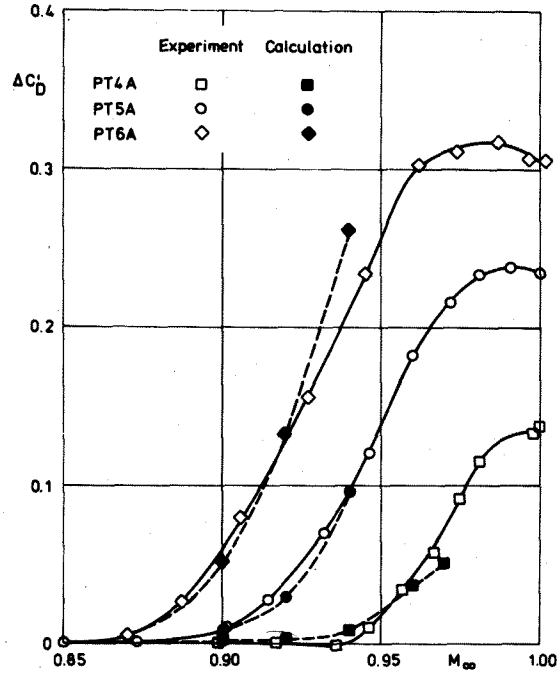

FIGURE 15. Comparison of experimental and theoretical drag-rise coefficients C_D' (nose drag subtracted) for the affinely related models PT4A, PT5A and PT6A

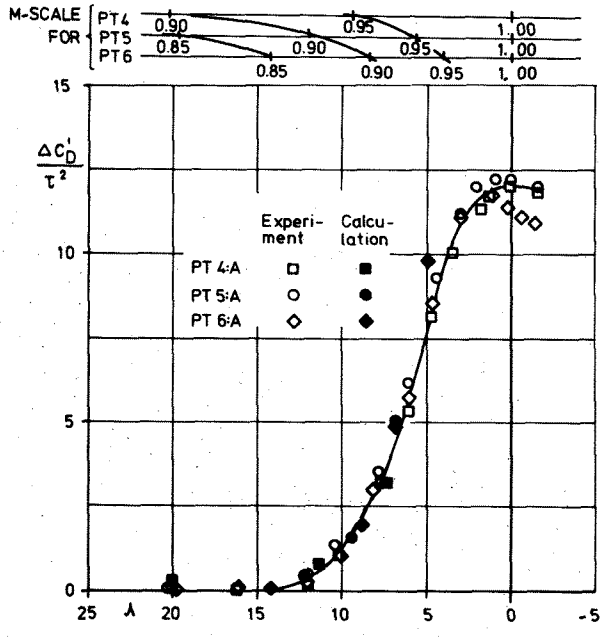

FIGURE 16. Verification of the transonic similarity concept from tests and computations for the three affinely related wing-body models

drag subtracted) versus Mach number for the affine wing-body family. Correspondingly corrected experimental data are included for comparative purposes. The agreement between theory and experiment is very good for the PT5A, whereas the slope of the calculated curve is a little bit lower than the experimental for PT4A and higher for PT6A. Boundary layer separation at the wing trailing edges shown in Figure 12 would probably have the effect of lowering the experimental curve.

Presented in Figure 16 is the calculated reduced drag-rise coefficient $\Delta C_D'/\tau^2$ versus the similarity parameter λ, and the experimental results are included for comparison. All data correlate very well and the validity of the transonic similarity concept for this kind of configurations is verified by the theoretical calculations as well as by the experiments.

Area Rule Investigation

Results for Models with Area Distribution 1 (B-family).. The transonic equivalence rule of Oswatitsch [20] and the transonic area-rule of Whitcomb [6] state that the drag at near sonic speed of a non-lifting slender body or a low-aspect ratio thin wing-body combination is primarily dependent on the axial cross-sectional area distribution. The drag is equal to that of the equivalent body of revolution whenever, according to Berndt [21] and others, the area distribution has zero slope at the rear end of the body or the body ends with an axisymmetric portion. The models in the family with area distribution 1 in the present test all have cylindrical afterbodies of the same diameter but the wings are not-so-thin and the aspect ratio not-so-low allowing investigation of the applicability of the area-rule for this kind of configuration.

Depicted in Figure 17 is the drag-rise coefficient ΔC_D versus Mach number for this model family. The reference area, which is the same for all models is the maximum cross sectional

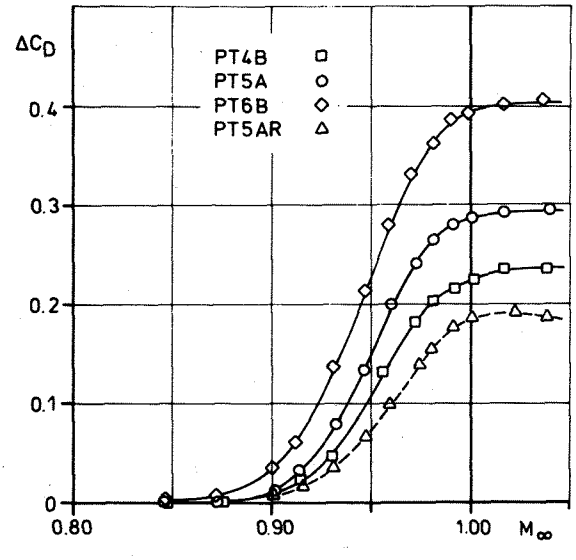

FIGURE 17. The experimental drag-rise curves for models with axial area distribution 1

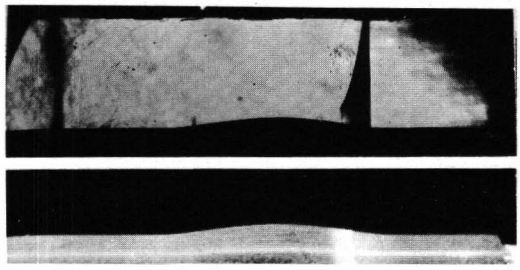

FIGURE 18a. PT5AR $M_\infty = 0.959$

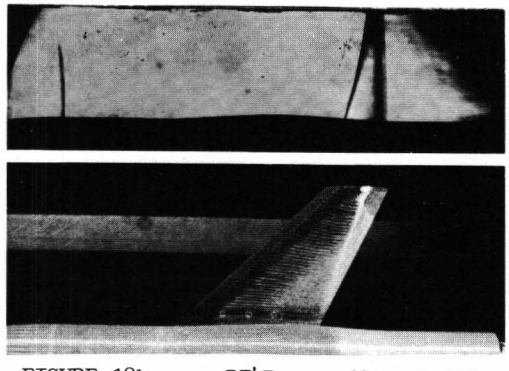

FIGURE 18b. PT4B $M_\infty = 0.959$

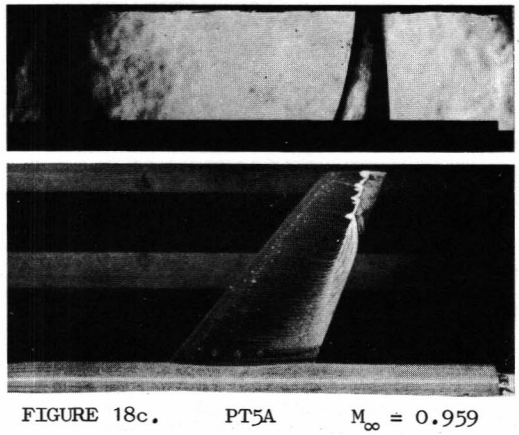

FIGURE 18c. PT5A $M_\infty = 0.959$

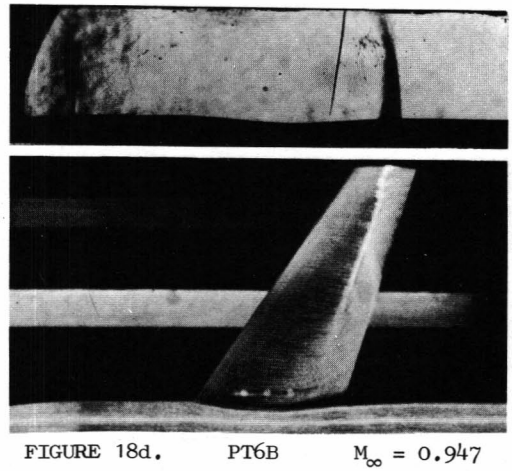

FIGURE 18d. PT6B $M_\infty = 0.947$

FIGURE 18. Schlieren and surface flow visualization pictures for the models with axial area distribution 1.

area. It is obvious that these configurations do not correlate at all with the transonic area-rule concept. Shown in Figure 18 are some Schlieren and oil flow pictures representing the Mach numbers around $M_\infty = 0.95$, where the boundary layer separations are most severe. At $M_\infty = 1.00$ the separations are limited to a narrow band close to the wing trailing edges for the configurations PT5A and PT6B. It is therefore not likely that the deviation from the area-rule to any large extent can be attributed to boundary layer effects.

Presented in Figure 19 is the calculated drag rise coefficient versus Mach number for the three wing-body combinations with area distribution 1. For comparative purposes the experimental results are included. Although the calculations have not been carried out at Mach numbers higher than $M_\infty = 0.94$, it is evident that the theoretical results do not correlate either with the transonic area-rule at speeds close to sonic. The agreement with the experimental data is fairly good, however. Oil flow studies at $M_\infty = 0.90$ reveal that at this Mach number there are no separations on any of the models, but that on PT6B the boundary layer flow at the wing surface near the trailing edge is largely directed towards the wing tip.

It is noteworthy that at the beginning of the drag-rise there is reasonable correlation between the lower aspect ratio models PT4B and PT5A in the theoretical and the experimental results, while the results for PT6B deviate practically at all points of the curve. This indicates that for this type of configurations simple "area-ruling" of the body could be an effective means to influence the critical Mach number, even if it is not effective at sonic speed.

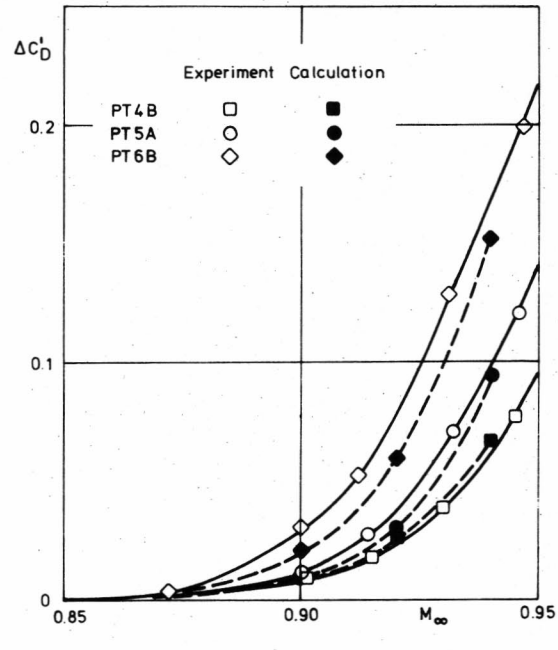

FIGURE 19. Comparison between measured and calculated drag-rise curves for models with axial area distribution 1

Results for Models with Area Distribution 4 (C-family). Shown in Figure 20 is the drag-rise coefficient ΔC_D versus Mach number for the C-family. It is apparent that for this family, which has a smoother and more favourable area distribution, the deviation from the transonic area-rule is generally even more marked than for the B-family except for the low aspect ratio model PT4C, which at low Mach numbers (around $M_\infty = 0.90$) correlates fairly well with the equivalent axisymmetric body PT5CR. From the oil-flow pictures in Figure 21 it can be observed that at the Mach number shown $M_\infty = 0.95$, the flow is attached on PT4C and PT5CR, while on PT5C and PT6C there are extensive areas of separated flow on the wing as well as at the body indentation. It might be inferred that the partly separated flow is the main reason for the deviation from the transonic area rule, but this is contradicted by the calculations as depicted in Figure 22, which show the same deviation from the area rule. The experimental drag-rise values for PT4C shown in Figure 22 are low, which might indicate that, as mentioned earlier, the nose drag correction is probably not adequate for the C-family and that consequently the very good agreement between calculated and experimental results for PT5C and PT6C is partly fortuitous. The trend is the same, however, in the calculated and in the experimental results, and it is therefore concluded that the transonic area-rule is not applicable for this family of wing-body combinations, except for the low aspect ratio configurations at Mach numbers in the beginning of the drag-rise curve.

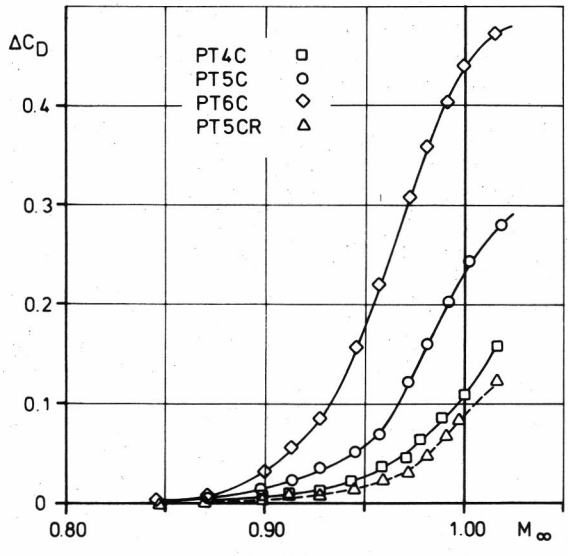

FIGURE 20. The experimental drag-rise curves for models with axial area distribution 4 (C-models)

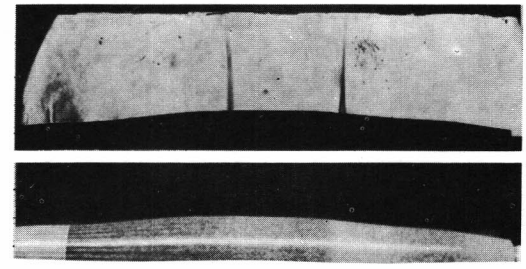

FIGURE 21a. PT5CR $M_\infty = 0.945$

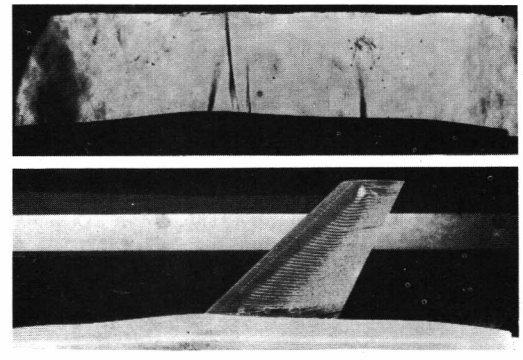

FIGURE 21b. PT4C $M_\infty = 0.945$

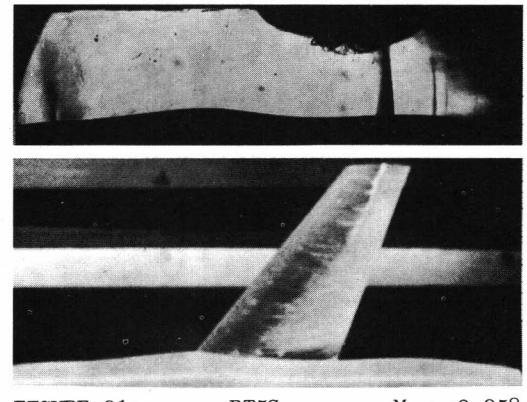

FIGURE 21c. PT5C $M_\infty = 0.958$

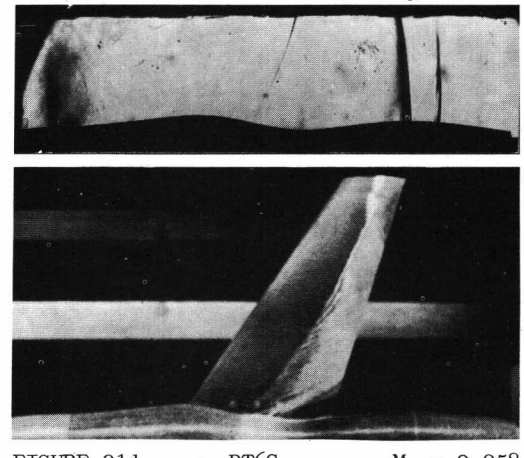

FIGURE 21d. PT6C $M_\infty = 0.958$

FIGURE 21. Schlieren and surface flow visualization pictures for the models with area distribution 4

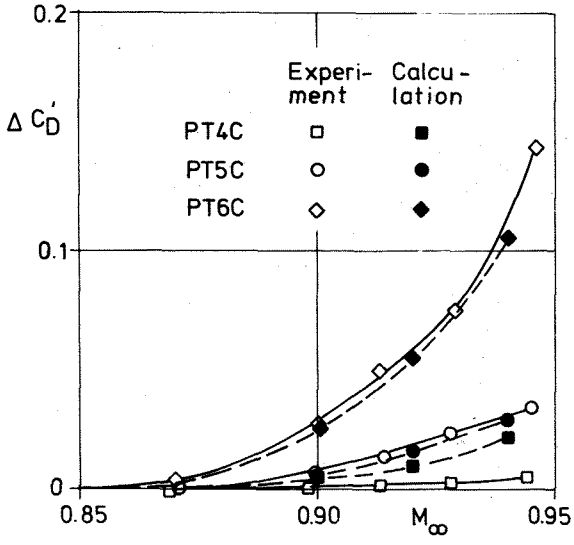

FIGURE 22. Comparison between measured and calculated drag-rise curves for wing-body models with axial area distribution 4 (C-models)

CONCLUDING REMARKS

The results of a theoretical and experimental investigation conducted to explore the applicability of the transonic similarity concept and of the transonic area-rule for non-slender trapezoidal swept wing-body combinations (wing aspect ratios 3-5) and their equivalent axisymmetric bodies at zero lift have shown that

- The transonic similarity rule for the flow around slender bodies is applicable for the investigated family of non-slender radially scaled wing-body combinations and also for their equivalent bodies of revolution.
- The transonic similarity rule for thin wings is applicable at sonic speed.
- The transonic area-rule is not valid at sonic speed for any of the wing-body combinations investigated. The lower aspect ratio models (A = 3-4) correlate reasonably well with the area-rule at Mach numbers in the lower end of the drag-rise curve.
- Drag rise coefficient calculated by the transonic small disturbance method shows good agreement with experimental data. The method seems to be a useful tool also for drag computations for fairly complicated wing-body combinations.

REFERENCES

1. Spreiter, J.R.
Aerodynamics of Wings and Bodies at Transsonic Speeds.
J. of the Aero/Space Sciences, Volume 26, Number 8, Aug 1959, p. 465-486 and p. 517.

2. Oswatitsch, K.
Similarity and Equivalence in Compressible Flow, Advances in Applied Mechanics.
Volume VI, edited by H.L. Dryden and Th. von Kármán, Academic Press, New York and London 1960, p. 153-271.

3. Oswatitsch, K.
Spezialgebiete der Gasdynamik.
Springer-Verlag, Wien, 1977, p. 124-146.

4. McDevitt, J.B.
A Correlation by Means of Transonic Similarity Rules of Experimentally Determined Characteristics of a Series of Symmetrical and Cambered Wings of Rectangular Plan Form.
NACA Report 1253, 1955.

5. Page, W.A.
Experimental Determination of the Range of Applicability of the Transonic Area Rule for Wings of Triangular Plan Form.
NACA TN 3872, 1956.

6. Whitcomb, R.T.
A Study of the Zero Lift Drag-Rise Characteristics of Wing-Body Combinations Near the Speed of Sound.
NACA Report 1273, 1956.

7. Drougge, G.
An Experimental Investigation of the Interference between Bodies of Revolution at Transonic Speeds with Special Reference to the Sonic and Supersonic Area Rules.
FFA Report 83, 1959, with special reference to the Appendix:

Berndt, S.B.
Hilding, L.O.
Application of the Transonic Principle of Equivalence to a Pair of Bodies of Revolution.

8. Guderley, K.G.
Theorie schallnaher Strömungen.
Springer-Verlag, Berlin/Göttingen/Heidelberg, 1957, Chapter 3, Section 4.

9. Oswatitsch, K.
The Area Rule.
Appl. Mech. Rev., Vol. 10, No. 12, Dec. 1957, p. 543-545.

10. Schmidt, W.
Hedman, S.
Recent Explorations in Relaxation Methods for Three-Dimensional Transonic Potential Flow.
ICAS Paper 76-22, Oct. 3-8, 1976.

11. Drougge, G.
Agrell, N.
Hedman, S.
Torngren, L.
Evaluation and Analysis of Computations and Experiments for Transonic Wing-Body Configurations.
ICAS Paper to be presented at 11th ICAS Congress, Lisbon, Portugal, Sept. 1978.

12. FFA Wind Tunnel Facilities.
FFA Memorandum 93, Stockholm 1974.

13. Torngren, L.
Investigation of Drag at Small Angles of Attack in the M-Range 0.5—1.0 for a Schematical Model of a Swept Wing Aircraft with Variation of the Area Distribution of the Body (in Swedish).
FFA AU-1018, Stockholm 1974.

14. Sörensén, H.
Atraghji, E.
Effect of Reynolds Number on Swept-Wing-Body Configurations with High Lift Devices at Transonic Speeds.
Paper at ICAS IX Congress, Haifa, Israel, August 25-30, 1974.

15. Murman, E.H.
Cole. J.D.
Calculation of Steady Transonic Flows.
AIAA J., Vol. 9, No. 1, Jan. 1971, pp. 114-121.

16. Murman, E.H.
Analysis of Embedded Shock Waves Calculated by Relaxation Methods.
Proceedings of AIAA Computation Fluid Dynamics Conference, Palm Springs, Calif., July 197 , pp. 27-40.

17. W. Schmidt,
Progress in Transonic Flow Computations Analysis and Design Methods for Three Dimensional Flows.
von Kármán Institute for Fluid Dynamics, Lecture Series and Computational Fluid Dynamics, March 15-19, 1976.

18. Spreiter, J.R.
On the Range of Applicability of the Transonic Area Rule.
NACA TN 3673, May 1956.

19. Mattsson, R.
Investigation of the Range of Applicability for Transonic Similarity.
Preliminary Wind Tunnel Test Results (in Swedish).
FFA Test Note AU-1213, Oct. 1976.

20. Oswatitsch, K.
Die Teoretischen Arbeiten Über Schallnahe Strömungen am Flugtechnischen Institut der Kungl. Tekniska Högskolan, Stockholm.
Proc. of the Eighth Int. Congress on Theoretical and Applied Mechanics, Istanbul (1952).

21. Berndt, S.B.
On the Drag of Slender Bodies at Sonic Speed.
FFA Report 70, 1956.

ACKNOWLEDGEMENTS

The work described in this paper has been carried out under contract from the Air Materiel Department of the Swedish Defence Materiel Administration (Contract No. AU-1213). The authors wish to record that essential contributions to this investigation have been made by colleagues at SAAB-SCANIA and at FFA, in particular by Professor Sune B. Berndt, whose deep knowledge and fruitful comments have been of great help.